Monthly Notices of the ROYAL ASTRONOMICAL SOCIETY

MNRAS **429**, 2287–2297 (2013) doi:10.1093/mnras/sts498

3D deflagration simulations leaving bound remnants: a model for 2002cx-like Type Ia supernovae*

M. Kromer,[1†] M. Fink,[2] V. Stanishev,[3] S. Taubenberger,[1] F. Ciaraldi-Schoolman,[1] R. Pakmor,[4] F. K. Röpke,[2] A. J. Ruiter,[1] I. R. Seitenzahl,[2] S. A. Sim,[5] G. Blanc,[6,7] N. Elias-Rosa[8] and W. Hillebrandt[1]

[1] *Max-Planck-Institut für Astrophysik, Karl-Schwarzschild-Str. 1, D-85748 Garching bei München, Germany*
[2] *Institut für Theoretische Physik und Astrophysik, Universität Würzburg, Emil-Fischer-Straße 31, D-97074 Würzburg, Germany*
[3] *CENTRA – Centro Multidisciplinar de Astrofísica, Instituto Superior Técnico, Av. Rovisco Pais 1, P-1049-001 Lisbon, Portugal*
[4] *Heidelberger Institut für Theoretische Studien, Schloss-Wolfsbrunnenweg 35, D-69118 Heidelberg, Germany*
[5] *Research School of Astronomy & Astrophysics, Mount Stromlo Observatory, Cotter Road, Weston ACT 2611, Australia*
[6] *INAF Osservatorio Astronomico di Padova, Vicolo dell'Osservatorio 5, I-35122 Padova, Italy*
[7] *Université Paris Diderot-Paris 7, Laboratoire APC, 10 rue Alice Domon et Léonie Duquet, F-75205 Paris cedex 13, France*
[8] *Institut de Cincies de l'Espai (IEEC-CSIC), Facultat de Cincies, Campus UAB, E-08193 Bellaterra, Spain*

Accepted 2012 November 26. Received 2012 November 21; in original form 2012 October 15

ABSTRACT

2002cx-like supernovae are a sub-class of sub-luminous Type Ia supernovae (SNe). Their light curves and spectra are characterized by distinct features that indicate strong mixing of the explosion ejecta. Pure turbulent deflagrations have been shown to produce such mixed ejecta. Here, we present hydrodynamics, nucleosynthesis and radiative-transfer calculations for a 3D full-star deflagration of a Chandrasekhar-mass white dwarf. Our model is able to reproduce the characteristic observational features of SN 2005hk (a prototypical 2002cx-like supernova), not only in the optical, but also in the near-infrared. For that purpose we present, for the first time, five near-infrared spectra of SN 2005hk from −0.2 to 26.6 d with respect to *B*-band maximum. Since our model burns only small parts of the initial white dwarf, it fails to completely unbind the white dwarf and leaves behind a bound remnant of $\sim$1.03 $M_{\odot}$ – consisting mainly of unburned carbon and oxygen, but also enriched by some amount of intermediate-mass and iron-group elements from the explosion products that fall back on the remnant. We discuss possibilities for detecting this bound remnant and how it might influence the late-time observables of 2002cx-like SNe.

Key words: hydrodynamics – radiative transfer – methods: numerical – techniques: spectroscopic – supernovae: individual: SN 2005hk.

1 INTRODUCTION

Due to an empirical relation between their peak brightness and their light-curve evolution (Pskovskii 1977; Phillips 1993), Type Ia supernovae (SNe Ia) can be used as standardizable candles to measure the expansion history of the Universe (Riess et al. 1998; Schmidt et al. 1998; Perlmutter et al. 1999). However, we still have no detailed picture about the progenitor systems of these luminous explosions beyond the general idea that they originate from the thermonuclear disruption of carbon–oxygen (CO) white dwarfs (WDs) (for a review, see e.g. Hillebrandt & Niemeyer 2000). Radioactive isotopes, in particular ^{56}Ni and its daughter nucleus ^{56}Co, which are synthesized within the thermonuclear burning, power the observable display of SNe Ia.

As of today several sub-classes of SNe Ia have been identified (Li et al. 2011). Among the most peculiar of these events are the SN 2002cx-like objects (Li et al. 2003). For their light-curve decline rate, these objects are sub-luminous with respect to the Phillips relation and do not show secondary maxima in the near-infrared (NIR) bands. Their spectra are characterized by very low expansion velocities compared to other SNe Ia and show signs of strong mixing in the ejecta (Jha et al. 2006; Phillips et al. 2007). This is in clear contrast to normal SNe Ia, which are characterized by strongly layered ejecta (Stehle et al. 2005; Mazzali et al. 2007).

While explosion models involving a detonation are not able to explain such an ejecta structure (e.g. Sim et al. 2010; Seitenzahl et al. 2012), such a strong mixing can easily be obtained from

*Based on observations collected at the European Southern Observatory (ESO), Paranal. Programme ID 076.D-0183
† E-mail: mkromer@mpa-garching.mpg.de

Published by Oxford University Press on behalf of the Royal Astronomical Society

turbulent deflagrations in WDs (Gamezo, Khokhlov & Oran 2004; Röpke & Hillebrandt 2005). The low expansion velocities are also in good agreement with the small amount of kinetic energy released in deflagration models. Such considerations led Branch et al. (2004) and Jha et al. (2006) to conclude that SN 2002cx-like objects might be related to pure deflagrations of Chandrasekhar-mass WDs. This interpretation was supported by Phillips et al. (2007), who compared the broad-band light curves of SN 2005hk (a well-sampled prototypical 02cx-like event) to synthetic light curves of a 3D deflagration model of Blinnikov et al. (2006) and found good agreement between the data and the model.

The models presented by Blinnikov et al. (2006), however, do not allow for a detailed comparison to the observed spectral time sequence since the multigroup approximation employed in their radiative-transfer simulations is too coarse. Moreover, their underlying hydrodynamic explosion models are restricted to one spatial octant of the progenitor WD, introducing artificial symmetries to the flame evolution. Here, we report on a 3D full-star deflagration simulation through to the homologous expansion phase. We perform detailed radiative-transfer calculations with the time-dependent 3D radiative-transfer code ARTIS (Sim 2007; Kromer & Sim 2009) from which we obtain a time series of synthetic spectra that we compare to the observed spectra of SN 2005hk.

The paper is organized as follows. In Section 2 we give a brief description of our explosion simulation and present the resulting ejecta structure. In Section 3 we present synthetic observables for this explosion model and compare them to the observed light curves and spectra of SN 2005hk. Finally, we discuss our results and give conclusions in Sections 4 and 5, respectively.

2 EXPLOSION SIMULATION

A Chandrasekhar-mass WD is believed to undergo about a century of convective carbon burning in the centre before a thermonuclear runaway finally sets in. Since this so-called simmering phase is characterized by highly turbulent flows, it cannot be fully accounted for by present-day numerical simulations (but see e.g. Höflich & Stein 2002; Kuhlen, Woosley & Glatzmaier 2006; Zingale et al. 2009; Nonaka et al. 2012). Thus, the actual ignition configuration of Chandrasekhar-mass WDs is not well constrained. Given this ignorance, one may use the ignition geometry as a free parameter and explore a larger set of explosion simulations with various ignition setups. Thereby one has to account for both different ignition strengths and ignition positions. A good way to achieve the former is to use a multispot ignition scheme which seeds unstable burning modes in a robust and numerically well-controlled way. Recently, we have performed such a systematic study for different ignition setups of 3D full-star pure deflagration simulations (Fink et al., in preparation) yielding ^{56}Ni masses between 0.035 and 0.38 $M_{\odot}$.

Here, we focus on a detailed comparison to SN 2005hk. For that purpose we select one of the models of the series by Fink et al. that produces a ^{56}Ni mass of the order of the observationally derived value of SN 2005hk. Applying Arnett's law (Arnett 1982) to the observed bolometric light curve, Phillips et al. (2007) report a ^{56}Ni mass of $\sim$0.2 $M_{\odot}$ for this SN. With a ^{56}Ni mass of 0.18 $M_{\odot}$, model N5def of the Fink et al. series comes close to that value.

In the N5def simulation, an isothermal ($T = 5 \times 10^5$ K) Chandrasekhar-mass WD was set up in hydrostatic equilibrium with a central density of 2.9×10^9 g cm^{-3} and a homogeneous composition of carbon and oxygen in equal parts by mass.[1] To account for an assumed solar metallicity of the zero-age main-sequence progenitor, we start with a Y_e of 0.498 86, corresponding to 2.5 per cent of ^{22}Ne in the initial composition. The WD was then discretized on a three-dimensional Cartesian moving grid (Röpke 2005) with 512^3 cells consisting of two nested parts (central resolution of 1.9 km) and ignited in five spherical ignition kernels that were placed randomly in a Gaussian distribution within a radius of 150 km from the WD's centre. By chance, for model N5def this algorithm produced a fairly one-sided ignition configuration with all kernels lying in a relatively small solid angle. Thus, this configuration is representative for a slightly off-centred single-spot ignition with a larger number of initially excited burning modes. The actual configuration is shown in Fig. 1. All kernels have a radius of $r_{\mathrm{ka}} = 10$ km and are at distances d between 6.3 and 80.9 km from the origin (see Table 1).

Neglecting any possible deflagration-to-detonation transition [see Seitenzahl et al. (2012) for an alternative evolution of this model in a delayed-detonation scenario] we followed the flame evolution up to

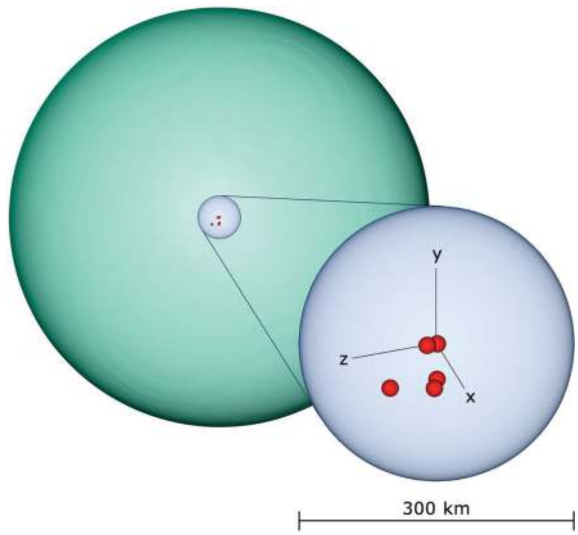

Figure 1. Ignition setup of the N5def model. Shown is a volume rendering of the WD in mint green colour. As discussed in Section 2, the ignition kernels were randomly placed within a radius of 150 km around the centre of the WD, as illustrated by the bluish sphere. The exact configuration of the ignition kernels is shown in the enlarged inlay (see also Table 1).

Table 1. Position of the ignition kernels of model N5def. Given are the x, y and z coordinates of the centre of the individual ignition kernels and their distance d to the centre of the WD.

#	x	y (in km)	z	d
1	65.5	−15.5	24.0	71.5
2	38.6	−22.7	67.3	80.9
3	13.0	8.2	15.1	21.6
4	−5.0	−51.3	−2.6	51.7
5	5.6	2.9	0.6	6.3

[1] Although the detailed flame evolution depends on the exact value of the central density (which is not well constrained for Chandrasekhar-mass WDs; e.g. Seitenzahl, Ciaraldi-Schoolmann & Röpke 2011), it is not expected to have a qualitative impact on the outcome of the explosion.

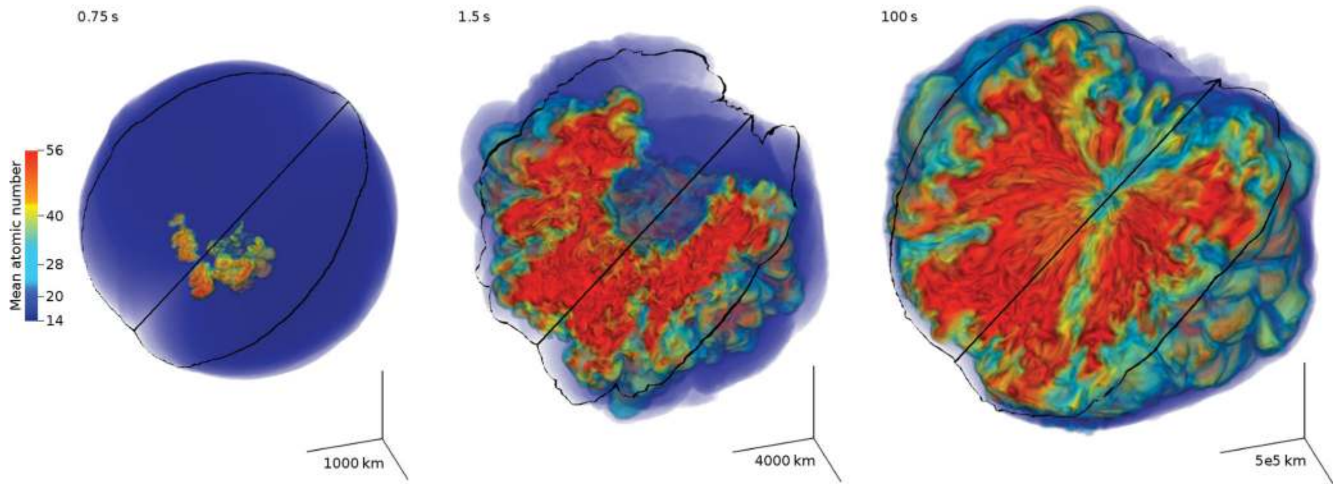

Figure 2. Snapshots of the hydrodynamic evolution of our model N5def. Shown are volume renderings of the mean atomic number calculated from the reduced set of species in the hydrodynamic simulation (see the colour bar). To allow a view to the central part of the ejecta, a wedge was carved out from the front of the ejecta. (i) At 0.75 s a one-sided deflagration plume rises towards the WD surface and fragments due to Rayleigh–Taylor and Kelvin–Helmholtz instabilities. (ii) At 1.5 s the expansion of the WD quenches the burning and the explosion ashes wrap around the unburned core. (iii) Finally, at 100 s the unburned core is completely engulfed by the explosion ashes which are ejected into space. The small triads at the bottom-right corner of each panel indicate the scaling at the origin of each plot: from left to right the legs of the triads represent 1000, 4000 and 500 000 km, respectively.

100 s after ignition when the ejecta reach homologous expansion. To this end we used the LEAFS code, a three-dimensional finite-volume discretization of the reactive Euler equations which is based on the PROMETHEUS implementation (Fryxell, Müller & Arnett 1989) of the 'piecewise parabolic method' by Colella & Woodward (1984). Deflagration fronts are modelled as discontinuities between CO fuel and nuclear ash, and their propagation is tracked with a level-set scheme (Smiljanovski, Moser & Klein 1997; Osher & Sethian 1988; Reinecke et al. 1999). All material crossed by these fronts is converted to nuclear ash with a composition and energy release depending on fuel density. Composition and energy release are interpolated from tables which have been calibrated using our full 384-isotope network. After a very short phase of laminar burning following ignition, the propagation of deflagrations is dominated by buoyancy-induced and shear-induced instabilities and interactions with a complex turbulent flow field. The unresolved acceleration of the flame due to turbulence is accounted for by a sub-grid-scale model (Schmidt, Niemeyer & Hillebrandt 2006a; Schmidt et al. 2006b). Self-gravity is dealt with by a monopole gravity solver.

The hydrodynamic evolution of our model is shown in Fig. 2. Since a deflagration flame cannot burn against the density gradient, our asymmetric ignition configuration leads to the formation of a one-sided deflagration plume that fragments due to Rayleigh–Taylor and Kelvin–Helmholtz instabilities. Once the deflagration front reaches the outer layers of the WD, the burning quenches due to the expansion of the WD and the ashes wrap around the still unburned core until they finally engulf it completely. A similar evolution of the deflagration flame was already described for single-spot off-centre ignitions by e.g. Plewa, Calder & Lamb (2004) and Röpke, Woosley & Hillebrandt (2007). While Plewa et al. (2004) found an ensuing detonation to be triggered when the ashes collide on the far side of the star (see also Seitenzahl et al. 2009a), we – similarly to Röpke et al. (2007) and Jordan et al. (2012b) – do not find high enough densities and temperatures for such a detonation to occur due to a significant expansion of the WD during the deflagration phase.

Since only a moderate fraction of the core of the WD is burned, the nuclear energy release in our simulation ($E_{\rm nuc} = 4.9 \times 10^{50}$ erg) is less than the binding energy of the initial WD ($E_{\rm bind} = 5.2 \times 10^{50}$ erg). Nevertheless, about 0.37 $M_\odot$ of the WD is accelerated to escape velocity and ejected into the ambient medium with a kinetic energy of 1.34×10^{50} erg. The remainder of the mass of the initial WD is left behind and forms a *bound remnant*. Similar findings were already reported in 2D (e.g. Livne, Asida & Höflich 2005) and recently in the context of a failed gravitationally confined detonation (Jordan et al. 2012b).

To obtain detailed nucleosynthesis yields of the explosion, we performed a post-processing calculation with a 384-isotope network for 10^6 Lagrangian tracer particles which were passively advected during the hydrodynamic simulation to record thermodynamic trajectories of mass elements (Travaglio et al. 2004; Seitenzahl et al. 2010). A compilation of the masses of important species is given in Table 2. To determine the mass that stays bound in the remnant and that of the unbound ejecta, we calculated the asymptotic specific kinetic energy $\epsilon_{\rm kin,\,a} = \epsilon_{\rm kin,\,f} + \epsilon_{\rm grav,\,f}$ for all tracer particles. Here, $\epsilon_{\rm kin,f} = v_{\rm f}^2/2$ and $\epsilon_{\rm grav,\,f}$ are the specific kinetic and gravitational binding energies at $t = 100$ s, i.e. at the end of our simulation,

Table 2. Yields of select species for model N5def.

	Bound remnant ($M_\odot$)	Ejecta ($M_\odot$)
Total	1.028	0.372
C	0.422	0.043
O	0.484	0.060
Ne	0.054	0.005
Mg	0.004	0.013
Si	0.015	0.025
S	0.004	0.009
Ca	0.0003	0.001
Fe	0.004	0.031
Ni	0.025	0.187
^{56}Ni	0.022	0.158

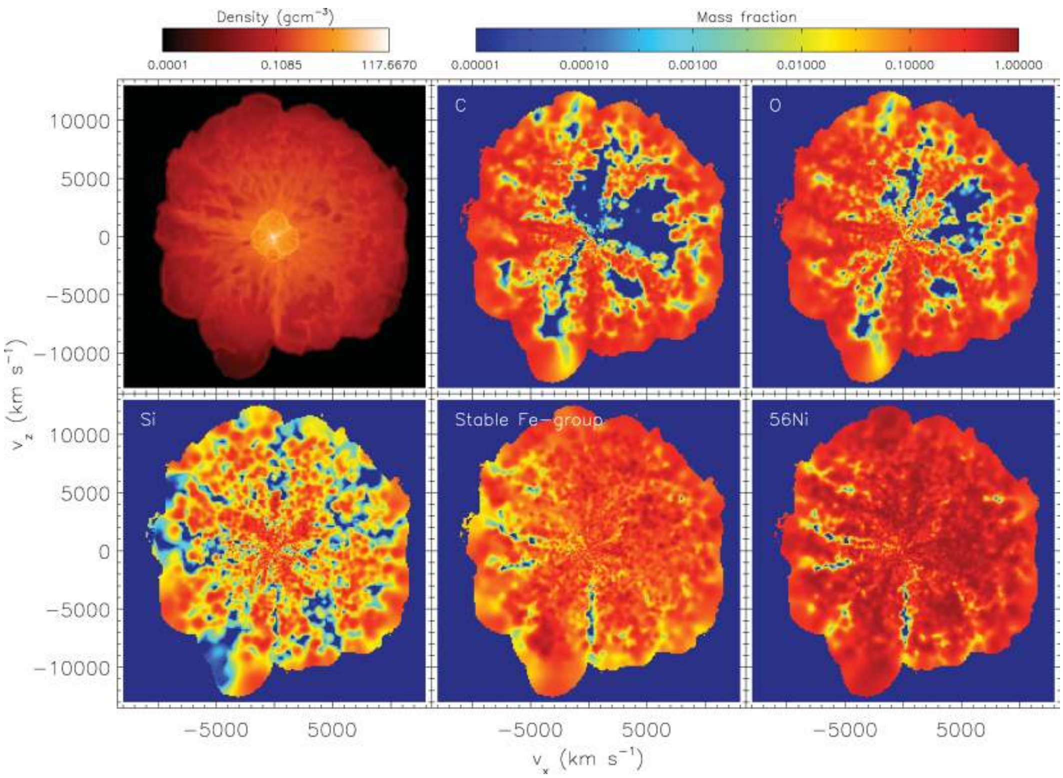

Figure 3. Composition of the unbound ejecta of model N5def. Shown are slices through the x–z plane in the asymptotic velocity space at 100 s after the explosion. The top-left panel displays the density, the following panels show the mass fraction of selected species (C, O, Si, stable iron-group elements and ^{56}Ni from top-left to bottom-right).

respectively. Only for positive values of $\epsilon_{\mathrm{kin,\,a}}$ a particle will be able to escape the gravitational potential. Otherwise, it will stay bound.

Finally, we mapped the unbound tracer particles to a Cartesian grid to reconstruct the chemical composition of the explosion ejecta in the asymptotic velocity space.[2] To this end, we used a smoothed particle hydrodynamic like algorithm as described in Kromer et al. (2010). The resulting ejecta structure is shown in Fig. 3. In contrast to the simulation by Jordan et al. (2012b), our model shows no pronounced large-scale composition asymmetry. There are, however, small-scale anisotropies due to the turbulent evolution of the deflagration flame. The density jump at about 2000 km s^{-1} is produced during the strongest pulsation of the bound core (at $t \sim 12$ s). After significant initial expansion due to burning, the mostly unburned inner parts of the ejecta start falling back inwards. This leads to the formation of a central compact core, which, after maximum compression, starts to expand again. At the same time, outer layers are still infalling and an accretion shock forms at the edge of the dense core (cf. Bravo & García-Senz 2009). In our model, maximum temperatures in the accretion shock just reach 10^9 K at densities of 5×10^5 g cm^{-3}; therefore, no detonation will be triggered (for critical conditions, see Röpke et al. 2007; Seitenzahl et al. 2009b).

3 SYNTHETIC OBSERVABLES

To obtain synthetic spectra and light curves for our model, we used the time-dependent 3D Monte Carlo radiative-transfer code ARTIS (Kromer & Sim 2009; Sim 2007). For the radiative-transfer simulation we mapped the abundance and density structure of the unbound ejecta at the end of the hydrodynamic simulations (by which point homologous expansion is a good approximation) to a 50^3 Cartesian grid and followed the propagation of 10^8 photon packets for 111 logarithmically spaced time steps between 2 and 120 d after explosion. To speed up the initial phase, a grey approximation, as discussed by Kromer & Sim (2009), was used in optically thick cells, and the initial 10 time steps (i.e. the initial three days after the explosion) were treated in local thermodynamic equilibrium. For our simulation we used the 'big_gf-4' atomic data set of Kromer & Sim (2009) with a total of $\sim 8.2 \times 10^6$ bound–bound transitions. The resulting broad-band light curves and a spectral time series are shown in Figs 4 and 5 and compared to SN 2005hk as a proxy for SN 2002cx-like objects.

3.1 Broad-band light curves

As reported by Jha et al. (2006) and Phillips et al. (2007), SN 2002cx-like objects are characterized by distinct spectral features and light curves. In the following, we will investigate to which extent our model is capable of reproducing these features. From the broad-band light curves in Fig. 4, it is immediately obvious that our model matches the *low-peak luminosities* of 2002cx-like SNe quite well. This, of course, is not so surprising, since we picked a model with a ^{56}Ni mass close to that observationally derived for SN 2005hk. However, we do not only get the correct peak luminosities but also approximately the right colours at maximum. Moreover, our model naturally explains the absence of secondary maxima in the NIR bands. This is a consequence of the turbulent burning, which leads to an almost completely mixed ejecta structure with

[2] For unbound tracer particles, the asymptotic velocity is determined as $v_{\mathrm{a}} = \sqrt{2\epsilon_{\mathrm{kin,a}}}$.

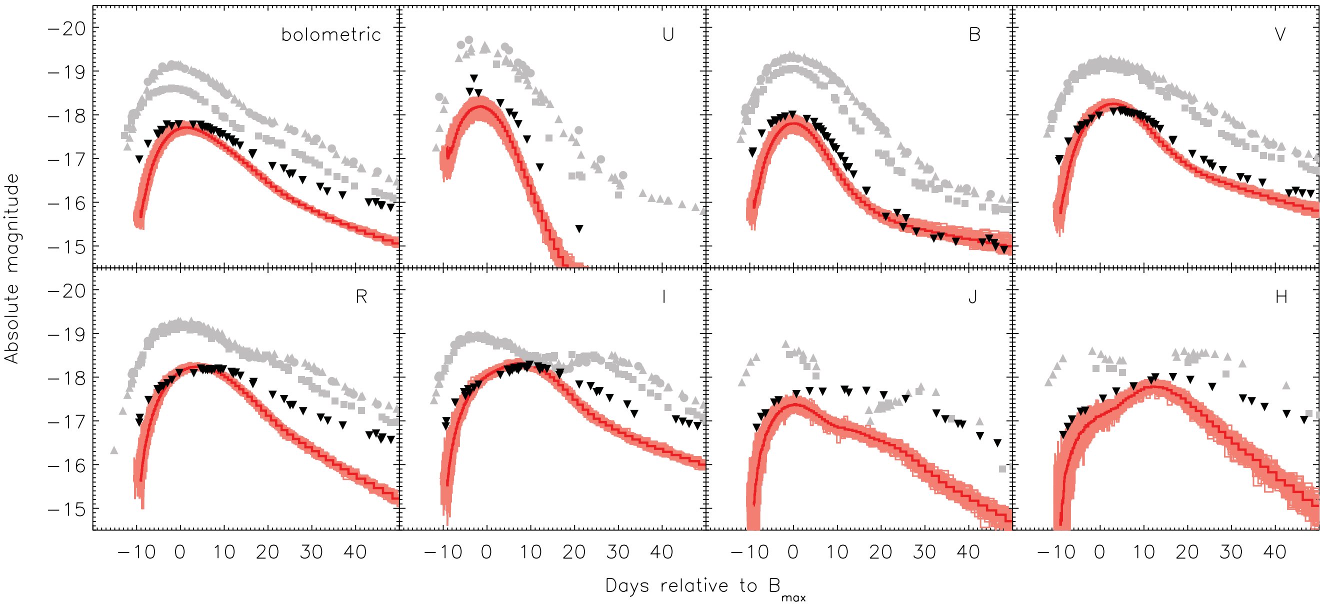

Figure 4. Synthetic light curves of our model. The panels from top-left to bottom-right contain *UBVRIJHK* bolometric and broad-band *U*, *B*, *V*, *R*, *I*, *J*, *H* light curves (Bessell & Brett 1988; Bessell 1990). The dark red line corresponds to the angle average of the model. The light red region indicates the scatter caused by 100 different viewing angles. Time is given relative to *B*-band maximum. The black upside-down triangles show the observed light curves of SN 2005hk (Phillips et al. 2007). Due to missing *K*-band data for SN 2005hk the bolometric light curve shown only accounts for *UBVRIJH* fluxes. For comparison, the grey symbols show observational data of three well-observed normal SNe Ia: SN 2003du (circles; Stanishev et al. 2007), SN 2004eo (squares; Pastorello et al. 2007a) and SN 2005cf (triangles; Pastorello et al. 2007b).

a roughly constant iron-group element (IGE) mass fraction at all velocities (see Figs 2 and 3). Kasen (2006) has shown that SN ejecta with such a homogenized composition are not expected to show secondary maxima in the NIR.

Other peculiarities of 2002cx-like SNe are their slowly declining light curves in *R* and redder bands and consequently also in *UVOIR* bolometric. In this respect our model has some shortcomings. While it nicely reproduces the post-maximum decline in the *U*, *B* and *V* bands, our post-maximum light-curve evolution is too fast particularly in *R* and redder bands, but also in *UVOIR* bolometric. This could be a consequence of our low ejecta mass of only 0.37 $M_{\odot}$, which is not able to trap enough γ-radiation after maximum. We note, however, that the synthetic light curves in Fig. 4 are only powered by radionuclides in the ejecta. Thereby we neglect any possible influence from the bound remnant, a puffed-up stellar object heated by the explosion, and also from the ^{56}Ni that falls back on to the remnant (see Table 2). After maximum light, when the ejecta start to become optically thin, the bound remnant will be exposed and it could kick in as an additional luminosity source. We will discuss this intriguing possibility in Section 4.3.

However, looking at the overall shape of the early light curves, an insufficient trapping of radiation in the ejecta and thus too low ejecta mass seem to be more likely. With a *B*-band rise time of 11.2 d, our model evolves somewhat too fast compared to the rise time of SN 2005hk, for which Phillips et al. (2007) find a value of 15 ± 1 d.

3.2 Optical spectra

Jha et al. (2006) and Phillips et al. (2007) also report peculiar features for the spectra of 2002cx-like SNe. At *pre-maximum epochs* they find an *SN 1991T-like spectrum* with a blue continuum, weak absorption features at $\sim$4200 and 5000 Å and no strong Ca II absorption features. As can be seen from the top panels of Fig. 5, our model naturally predicts this behaviour, characteristic of an ionization state higher than in normal SNe Ia.

Moreover, 2002cx-like SNe show a significant contribution from IGEs to the spectra at all epochs, while normal SNe Ia do not show strong IGE features until well after maximum light. Due to the strong mixing of the ejecta, our model is almost homogenized and thus predicts strong IGE contributions at all epochs. This is illustrated in Fig. 6. There, the colour coding below the synthetic spectrum indicates the fraction of escaping packets in each wavelength bin that were last emitted by bound–bound transitions of a particular element (the associated atomic numbers are illustrated in the colour bar). From this it is clearly visible that emission by IGEs already dominates the spectrum before maximum light, while this is not the case for stratified models, such as e.g. W7 (see fig. 2 of Kromer & Sim 2009).

Another characteristic feature of the spectra of 2002cx-like SNe is extremely low line velocities at all epochs, indicating significantly lower expansion velocities and thus less kinetic energy than in normal SNe Ia. Since our model burns only parts of the WD, the kinetic energy is rather low compared to other explosion models that fully burn and unbind the progenitor WD. As a consequence, the line velocities of our model are in good agreement with the observed ones (compare Fig. 5).

3.3 Near-infrared spectra

In Fig. 7 we show, for the first time, NIR spectra of a 2002cx-like SN. These spectra of SN 2005hk were collected by the European Research Training Network (RTN) 'The Physics of Type Ia Supernova Explosions'[3] (details on the observations and data reduction are given in Appendix A). Compared to normal SNe Ia there are a

[3] http://www.mpa-garching.mpg.de/~rtn/

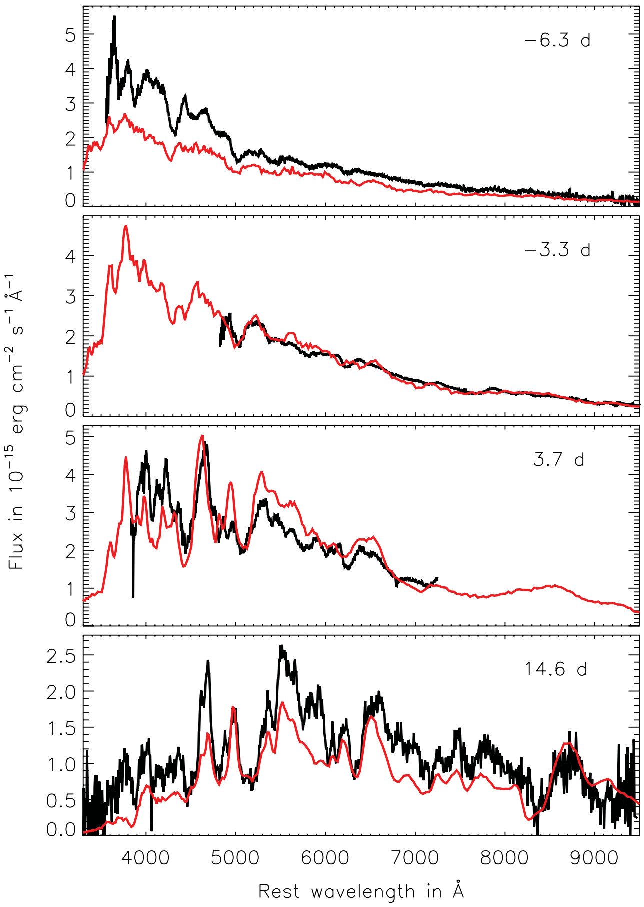

Figure 5. Spectral evolution of model N5def from −6.3 to 14.6 d (epochs are given with respect to *B*-band maximum). For comparison the observed spectra of the 2002cx-like SN 2005hk (Phillips et al. 2007) are overplotted in black. The observations were dereddened and deredshifted according to the values of Phillips et al. (2007) and Sahu et al. (2008), respectively.

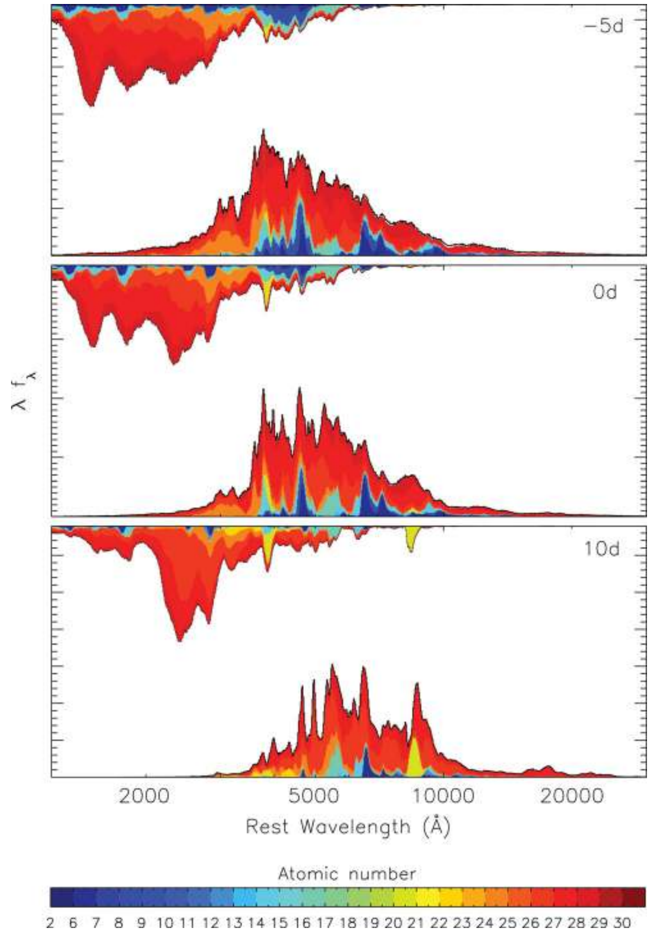

Figure 6. Formation of the UV-to-NIR SED for our N5def model for three different snapshots. Epochs are given relative to *B*-band maximum. The colour coding indicates the elements responsible for both bound–bound emission and absorption of quanta in the Monte Carlo simulation. The region below the synthetic spectrum is colour coded to indicate the fraction of escaping quanta in each wavelength bin that were last emitted by a particular element (the associated atomic numbers are illustrated in the colour bar). Similarly, the coloured regions along the top of the plots indicate which elements were last responsible for removing quanta from a particular wavelength bin (either by absorption or scattering/fluorescence). White regions between the emerging spectrum and the colour-coded bound–bound emission indicate the contribution of continuum processes (bound–free, free–free) to the last emission.

few prominent differences. While in normal SNe Ia the characteristic Co II emission humps in the *K* band (e.g. Gall et al. 2012) do not form before 20 d after maximum light, they emerge at 6.6 d after maximum in SN 2005hk (see the grey highlighted region in Fig. 7). At later epochs (∼30 d) the Co II features appear significantly more narrow in SN 2005hk than in normal SNe Ia. A similar but even stronger effect can be observed in the *J* and *H* bands, where very narrow spectral features develop at these epochs.

Our model naturally reproduces these characteristic features of the NIR spectra of SN 2005hk. The narrow features at later epochs are a direct consequence of the low kinetic energy released during the explosion and reflect the low expansion velocities of the ejecta (Fig. 3) compared to that of models of normal SNe Ia (e.g. Nomoto, Thielemann & Yokoi 1984, Röpke et al. 2012). The early occurrence of the Co II emission humps can be understood as a result of the almost completely mixed ejecta. While IGEs are concentrated in a central core in models of normal SNe Ia, the turbulent burning of our deflagration model leads to a very homogeneous IGE distribution in the ejecta, which extends to the highest velocities. As shown by Kasen (2006), such a mixing does not only lead to single-peaked NIR light curves but also lead to an increased NIR flux around *B*-band maximum.

Although our synthetic NIR spectra reproduce the characteristic features of SN 2005hk, a detailed comparison shows some differences. While the absolute flux level and the overall SED agree quite well with the observations around maximum light, differences start to emerge about a week after maximum light. At these epochs, the flux level of our model is too low compared to the observations as already discussed for the broad-band light curves (Section 3.1).

4 DISCUSSION

4.1 Spectropolarimetry

There are a few observational constraints which we cannot address directly with our synthetic observables. Chornock et al. (2006) and Maund et al. (2010) presented spectropolarimetric observations of SN 2005hk and reported a line and continuum polarization on a level of a few tenths of a percent, which is typical of SNe Ia (Wang & Wheeler 2008) and requires approximately spherical explosion

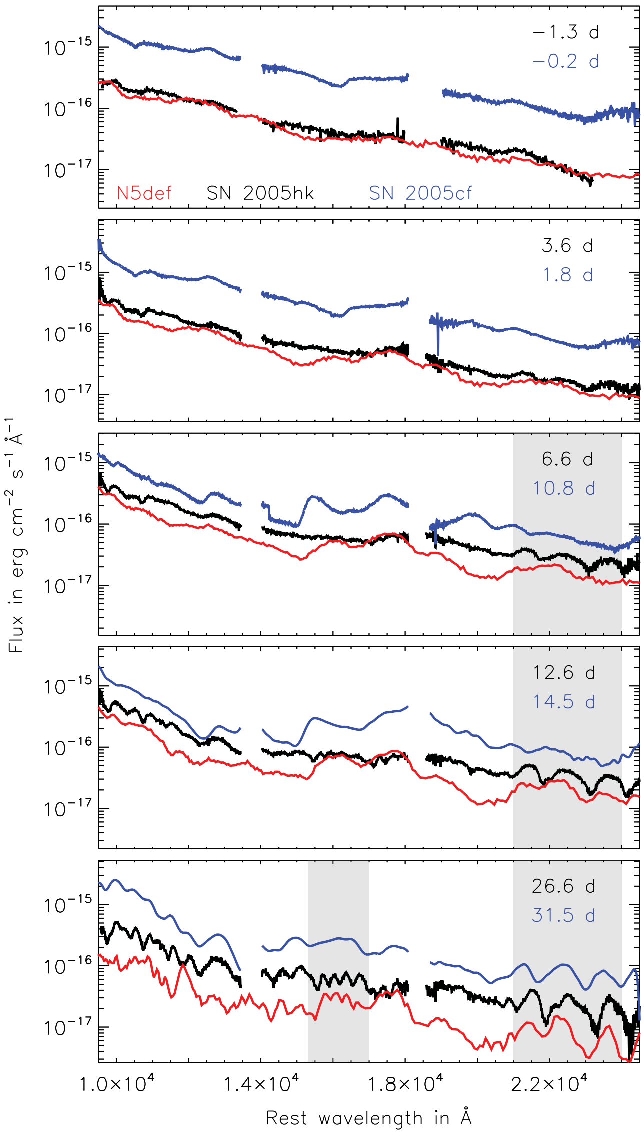

Figure 7. NIR spectra of the 2002cx-like SN 2005hk (black) and synthetic spectra of model N5def (red) from −1.3 to 26.6 d (epochs are given with respect to *B*-band maximum). The observations were dereddened and deredshifted according to the values of Phillips et al. (2007) and Sahu et al. (2008), respectively. For comparison, NIR spectra of the normal SN Ia 2005cf (Gall et al. 2012) are shown for similar epochs (blue).

ejecta. Since our radiative-transfer simulations currently do not include the polarization state of the radiation field, we cannot directly compare the observed polarization spectra to our model. We note, however, that our ejecta structure does not show very pronounced large-scale asymmetries (see Fig. 3) and that the synthetic observables are not very sensitive to different lines of sight as visible from the light curves in Fig. 4. Thus, a weak polarization signal seems plausible.

4.2 Late-time spectra

Further observational constraints come from late-time (approximately nine months after explosion) spectra, where 2002cx-like SNe show extremely narrow permitted Fe II lines and a continuum or pseudo-continuum-like SED (Jha et al. 2006; Phillips et al. 2007). In contrast, normal SNe Ia are in the nebular phase at these epochs. Jha et al. (2006) also report a tentative detection of weak O I features in the late-time spectra of SN 2002cx. They do, however, not see strong features of [O I] λλ6300, 6364 which have been predicted for 3D deflagration models (Kozma et al. 2005), where unburned O is present down to the lowest ejecta velocities due to turbulent burning as in our model.

Since ARTIS does not yet account for non-thermal ionization and excitation, which are the dominant processes at late epochs (e.g. Kozma & Fransson 1998a,b), we cannot directly test the late-time spectra of our models against the observations. Whether [O I] features will arise, however, depends strongly on a possible microscopic mixing of different species. This cannot be addressed with present-day numerical models, since it takes place on scales which are not resolved. However, if such a mixing is present, transitions of other species stronger than [O I] λλ6300, 6364 will dominate the cooling. Also the central density of our explosion ejecta (∼120 g cm^{-3} at 100 s after explosion) is about 30 times larger than in the W7 model (∼4 g cm^{-3}; Nomoto et al. 1984) or typical delayed-detonation models that are in good agreement with normal SNe Ia. This might be important in explaining the peculiar features of the late-time spectra of 2002cx-like SNe.

Beyond that, we can only speculate that the bound remnant in our model might be able to explain the peculiar non-nebular features of the late-time spectra of 2002cx-like SNe if the observed spectrum was a superposition of emission from the bound remnant and the SN ejecta. We will discuss the implications of the bound remnant in more detail in the next section. Alternatively, Sahu et al. (2008) tried to explain the observed late-time spectra of SN 2005hk by combining synthetic photospheric (e.g. Mazzali & Lucy 1993) and nebular (e.g. Mazzali et al. 2001) spectra of the ejecta of a parametrized 1D explosion model.

4.3 Implications of the bound remnant

As discussed in Section 2, our model does not burn the complete WD but leaves behind a bound remnant. Due to the strong expansion of the ejecta, at late times this remnant cannot be resolved from our simulations, thus preventing any detailed analysis. However, it is clear that the remnant must be a puffed-up stellar object heated during the explosion. From the bound tracer particles we can derive the overall composition of the remnant (see Table 2), which shows that it is enriched with IGE material and some amount of radioactive ^{56}Ni. This enrichment is due to fallback of explosion ashes on to the bound remnant, so that the enriched material should be located in the outer layers of the remnant (see also Jordan et al. 2012b).

We also note that the ^{56}Ni content of the bound remnant is large enough to contribute to the optical display of SN 2005hk at late epochs (Fig. 8) if γ-rays are completely trapped in the remnant. Since the remnant does not expand, its densities are significantly larger than those of the ejecta, making this assumption plausible. Having some contribution from the bound remnant at late epochs could also explain the highly peculiar spectra of 2002cx-like SNe, which never become fully nebular (see the discussion in the previous section). In particular, the extremely narrow IGE features might be explained if the emission originated from an IGE-rich crust of the bound remnant.

Being heated by the actual explosion and long-lived radioactive isotopes, the bound remnant might even become directly detectable at much later epochs when the explosion ejecta go into the SN remnant phase. For SN 2005hk, observations were performed with the Gran Telescopio Canarias (GTC) on 2012 July 20, i.e. 2443.5 d after *B*-band maximum. These, however, have not shown any point

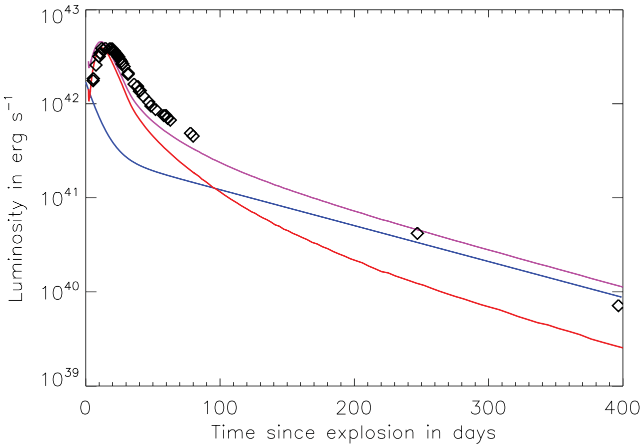

Figure 8. Bolometric light curve of SN 2005hk [black diamonds; following Phillips et al. (2007), we adopted a rise time of 15 d]. For comparison, the red line shows the synthetic bolometric light curve from our radiative-transfer simulation in the ejecta. At $t = 120$ d our detailed non-grey radiative-transfer simulation ends. Thereafter, we extended the synthetic light curve with a calculation using a grey *UVOIR* opacity. The blue curve shows the instantaneous energy deposition due to the ^{56}Ni decay sequence in the bound remnant, assuming full γ-ray trapping. The magenta curve shows the sum of both these contributions.

source down to a limiting magnitude of $M_r = -8.08 \pm 0.49$ (for details of the observation see Appendix B).

After the bound remnant has radiated away all the heat from the explosion and possible reheating from radioactive isotopes, it will again become a WD, however with a peculiar composition enriched in IGEs (and also intermediate-mass elements). Moreover, Jordan et al. (2012b) report kick velocities of up to 520 km s^{-1} for the remnant WDs in their failed gravitationally confined detonation simulations, thus claiming the existence of hypervelocity enriched WDs as a 'smoking gun' for this scenario. From our simulations we do not see such kicks. This difference may originate from the different gravity solvers used. In general, no perfect momentum conservation is to be expected from approximate solutions of the Poisson equation.

4.4 Implications on the binary companion star

One problem of single-degenerate progenitor models discussed in the literature is that of the non-detection of hydrogen lines in the observed (nebular) spectra of SNe Ia (e.g. Leonard 2007). Recent hydrodynamical simulations investigating the impact of SN Ia ejecta on a non-degenerate companion star (e.g. Liu et al. 2012; Pan, Ricker & Taam 2012) have shown that the amount of hydrogen stripped from the companion star seems to be significantly larger than the observationally derived upper limits (Leonard 2007). Due to the low kinetic energy of our explosion model, compared to that of normal SNe Ia, only a small amount of material should be stripped from the companion in the progenitor systems of SN 2002cx-like SNe, thus probably avoiding a signature of hydrogen lines in late-time spectra. This should be addressed by detailed impact studies in the future.

4.5 The class of 2002cx-like SNe

After the discovery of SN 2002cx by Li et al. (2003) as a peculiar object, it soon became evident that this was not a unique event but rather the prototype of a new class of peculiar SNe Ia with a striking spectral homogeneity (Jha et al. 2006). From a volume-limited sample of the Lick Observatory Supernova Search (LOSS), Li et al. (2011) estimate that SN 2002cx-like explosions contribute at about 5 per cent to the total SN Ia rate.

Recently, SN 2008ha (Foley et al. 2009) and SN 2007qd (McClelland et al. 2010) were proposed as additional members of the class. Though spectroscopically similar to SN 2002cx, those objects are fainter by more than 2 mag than a typical 2002cx-like SN and show far lower line velocities, of the order of 2000 km s^{-1}, while SNe 2002cx and 2005hk showed line velocities of the order of 7000 km s^{-1}. Nevertheless, McClelland et al. (2010) found a relationship between light-curve stretch, the peak brightness and the expansion velocities among their (small) sample of objects. This indicates that their extended class of SN 2002x-like objects may originate from a single explosion mechanism.

With an observationally derived ^{56}Ni mass of 0.003 $M_\odot$ for SN 2008ha (Foley et al. 2009), however, this object cannot easily be explained in our model of a deflagration of a Chandrasekhar-mass WD. From a systematic study of 3D full-star pure deflagration simulations for different ignition setups (Fink et al., in preparation), we obtain a minimum ^{56}Ni mass of 0.035 $M_\odot$, which is more than a factor of 10 larger than the observationally derived value for SN 2008ha. Though we did not sample all possible ignition setups in the Fink et al. study nor take into account different progenitor compositions, this difference may be difficult to reconcile with a deflagration of a Chandrasekhar-mass WD. Thus, another explosion mechanism might be at work for these faint objects. Foley et al. (2009, 2010) suggested deflagrations of sub-Chandrasekhar-mass WDs, while Valenti et al. (2009) and Moriya et al. (2010) favoured a core-collapse origin.

4.6 Rates

As mentioned in the previous section, Li et al. (2011) estimate from the LOSS that 2002cx-like SNe contribute at about 5 per cent to the total SN Ia rate. This is remarkably close to some theoretical predictions for the contribution of single-degenerate hydrogen-accreting systems to the total SN Ia rate. From binary population synthesis models, e.g. Ruiter, Belczynski & Fryer (2009) find a value of ~3 per cent (their model 1 with $\alpha_{\rm CE} \times \lambda = 1$). At the same time their predicted total SN Ia rate for all progenitor channels considered (single-degenerate Chandrasekhar-mass scenario and double-degenerate mergers with a total mass above the Chandrasekhar limit) is comparable to the Galactic SN Ia rate (Ruiter et al. 2009, fig. 2). Taking this at face value, it could be that all single-degenerate systems will end up as 2002cx-like SNe. Normal SNe Ia would then originate from other progenitors like double-degenerate mergers (e.g. Pakmor et al. 2012; Ruiter et al. 2012) or sub-Chandrasekhar-mass double detonations (e.g. Fink et al. 2010; Kromer et al. 2010; Woosley & Kasen 2011). However, the observationally derived SN rates as well as the binary population synthesis rate predictions for the single-degenerate scenario are somewhat uncertain. For example, Han & Podsiadlowski (2004) can reconcile the observed Galactic SN Ia rate with the birth rate of SNe Ia in the single-degenerate Chandrasekhar-mass scenario from calculations with their binary population synthesis code which assumes a different prescription for hydrogen accretion than Ruiter et al. (2009).

4.7 The fate of Chandrasekhar-mass explosions

In a companion study (Fink et al., in preparation) we are currently investigating the outcome of a larger set of 3D deflagration models.

Within this sample we find a wide range of explosion strengths depending on the actual ignition conditions. However, to obtain ^{56}Ni masses of the order of those derived for SN 2002cx or SN 2005hk, only a very narrow range of ignition configurations works.

We find that appropriate deflagrations with moderate ^{56}Ni production result from ignition setups that can be interpreted in the scheme of a slightly off-centre single-spot ignition. Thus, if all Chandrasekhar-mass explosions led to 2002cx-like SNe, as hypothesized in the previous section, only such ignition configurations should be realized in nature. Note that this is in agreement with state-of-the-art pre-ignition simulations (e.g. Kuhlen et al. 2006; Zingale et al. 2009; Nonaka et al. 2012).

However, it could also be that for other configurations an ensuing detonation after the initial deflagration phase occurs, thereby producing a layered ejecta structure as needed for normal SNe Ia (e.g. Mazzali et al. 2007). Several mechanisms to trigger such a secondary detonation have been proposed: a spontaneous deflagration-to-detonation transition (Khokhlov 1991), a gravitationally confined detonation (Plewa et al. 2004), a pulsating reverse detonation (Bravo & García-Senz 2006) or a pulsationally assisted gravitationally confined detonation (Jordan et al. 2012a). However, for none of these models the formation of the secondary detonation can be resolved in detail. Instead, detonations are triggered when certain conditions are met which are thought to be sufficient to ignite a detonation from simplified 1D simulations.

5 CONCLUSION

We have presented hydrodynamic simulations and radiative-transfer calculations for a 3D pure deflagration of a Chandrasekhar-mass WD. Our particular model (N5def), chosen from a larger sample of simulations (Fink et al., in preparation), has an asymmetric ignition configuration leading to a relatively weak deflagration, which fails to completely unbind the WD. Only $\sim$0.37 $M_\odot$ of material is ejected, whereas the remainder stays gravitationally bound, leaving behind a stellar remnant of $\sim$1 $M_\odot$.

The ejecta contain a significant ^{56}Ni mass ($\sim$0.16 $M_\odot$), have low kinetic energy, are well mixed and relatively symmetric on large scales. All of these properties make N5def a promising model for 2002cx-like SNe Ia. Moreover, a comparison of our synthetic observables with SN 2005hk shows good agreement. Our synthetic light curves reproduce the peak luminosity and colour of SN 2005hk and naturally predict the lack of a secondary maximum in the NIR bands. Our synthetic spectra are also in good agreement with observations. At optical wavelengths, N5def shows the same high ionization, low expansion velocities and early dominance of IGE lines observed in SN 2005hk. In addition, we have presented and compared with previously unpublished NIR spectra of SN 2005hk, allowing us to verify that the good match between model and observations extends into the NIR regime. The main shortcoming of the model is an overly rapid post-maximum fading at red and NIR wavelengths that is also apparent in the bolometric light curve, which is too narrow. This points at too low opacities, which could be the result of insufficient ejected mass.

The most intriguing feature of the model presented here is the bound remnant. Unfortunately, at late times the remnant is not resolved in the simulation, so that its exact state after the explosion remains largely unknown. We do find, however, that some fallback of nucleosynthetically processed material (including $\sim$0.02 $M_\odot$ of ^{56}Ni) on to the remnant will occur, resulting in a peculiar IGE-rich composition of the remnant object. Heated by the explosion, this will be a puffed-up stellar object. We can also speculate that the bound remnant may be sufficiently luminous to contribute to the observed display of the SN, explaining in part the highly peculiar late-time spectra of 2002cx-like SNe, which do not become fully nebular even 1 yr after the explosion.

While N5def seems to be a reasonable model for 2002cx-like SNe with ^{56}Ni masses of $\sim$0.2 $M_\odot$, it appears unlikely to produce ^{56}Ni masses two orders of magnitude lower in the deflagration of a Chandrasekhar-mass WD. These would be needed to explain 2008ha-like SNe, which have been suggested to be fainter and less energetic siblings of 2002cx-like SNe, originating from the same explosion mechanism.

Finally, we point out that the observed rate of 2002cx-like SNe (about 5 per cent of the total SN Ia rate) is quite similar to the contribution of the single-degenerate Chandrasekhar-mass explosion channel to the total SN Ia rate as expected from some binary population synthesis calculations. It is thus tempting to speculate that deflagration-to-detonation transitions might actually not happen in SNe Ia, and that single-degenerate Chandrasekhar-mass explosions might only lead to pure deflagrations with a 2002cx-like optical display.

ACKNOWLEDGMENTS

This work was supported by the European Union's Human Potential Programme 'The Physics of Type Ia Supernovae' under contract HPRN-CT-2002-00303, the Deutsche Forschungsgemeinschaft via the Transregional Collaborative Research Center TRR 33 'The Dark Universe', the Excellence Cluster EXC153 'Origin and Structure of the Universe' and the Emmy Noether Programme (RO 3676/1-1). MK, MF, FKR and SAS also acknowledge financial support by the Group of Eight/Deutscher Akademischer Austausch Dienst (Go8/DAAD) exchange programme. FKR is supported by the ARCHES prize of the German Ministry of Education and Research (BMBF).

The simulations presented in this work were carried out at the John von Neumann Institute for Computing in Jülich (Germany) as part of projects hmu20 and pra026 within the Partnership for Advanced Computing in Europe (PRACE).

This work makes use of data collected at the 8.2 m Very Large Telescope (Cerro Paranal, Chile; programme ID 076.D-0183) and the 10.4 m Gran Telescopio Canarias (La Palma, Spain; programme ID GTC19-12A).

REFERENCES

Adelman-McCarthy J. K. et al., 2008, ApJS, 175, 297
Arnett W. D., 1982, ApJ, 253, 785
Bessell M. S., 1990, PASP, 102, 1181
Bessell M. S., Brett J. M., 1988, PASP, 100, 1134
Blinnikov S. I., Röpke F. K., Sorokina E. I., Gieseler M., Reinecke M., Travaglio C., Hillebrandt W., Stritzinger M., 2006, A&A, 453, 229
Branch D., Baron E., Thomas R. C., Kasen D., Li W., Filippenko A. V., 2004, PASP, 116, 903
Bravo E., García-Senz D., 2006, ApJ, 642, L157
Bravo E., García-Senz D., 2009, ApJ, 695, 1244
Chornock R., Filippenko A. V., Branch D., Foley R. J., Jha S., Li W., 2006, PASP, 118, 722
Colella P., Woodward P. R., 1984, J. Comput. Phys., 54, 174
Fink M., Röpke F. K., Hillebrandt W., Seitenzahl I. R., Sim S. A., Kromer M., 2010, A&A, 514, A53
Foley R. J. et al., 2009, AJ, 138, 376
Foley R. J., Brown P. J., Rest A., Challis P. J., Kirshner R. P., Wood-Vasey W. M., 2010, ApJ, 708, L61

Fryxell B. A., Müller E., Arnett W. D., 1989, Hydrodynamics and Nuclear Burning. MPA Green Report 449, Max-Planck-Institut für Astrophysik, Garching
Fukugita M., Ichikawa T., Gunn J. E., Doi M., Shimasaku K., Schneider D. P., 1996, AJ, 111, 1748
Gall E. E., Taubenberger S., Kromer M., Sim S. A., Benetti S., Blanc G., Elias-Rosa N., Hillebrandt W., 2012, MNRAS, 427, 994
Gamezo V. N., Khokhlov A. M., Oran E. S., 2004, Phys. Rev. Lett., 92, 211102
Han Z., Podsiadlowski P., 2004, MNRAS, 350, 1301
Hillebrandt W., Niemeyer J. C., 2000, ARA&A, 38, 191
Höflich P., Stein J., 2002, ApJ, 568, 779
Jha S. et al., 2006, AJ, 131, 527
Jordan G. C. IV, et al., 2012a, ApJ, 759, 53
Jordan G. C. IV, Perets H. B., Fisher R. T., van Rossum D. R., 2012b, ApJL, 761, L23
Kasen D., 2006, ApJ, 649, 939
Khokhlov A. M., 1991, A&A, 245, 114
Kozma C., Fransson C., 1998a, ApJ, 496, 946
Kozma C., Fransson C., 1998b, ApJ, 497, 431
Kozma C., Fransson C., Hillebrandt W., Travaglio C., Sollerman J., Reinecke M., Röpke F. K., Spyromilio J., 2005, A&A, 437, 983
Kromer M., Sim S. A., 2009, MNRAS, 398, 1809
Kromer M., Sim S. A., Fink M., Röpke F. K., Seitenzahl I. R., Hillebrandt W., 2010, ApJ, 719, 1067
Kuhlen M., Woosley S. E., Glatzmaier G. A., 2006, ApJ, 640, 407
Leonard D. C., 2007, ApJ, 670, 1275
Li W. et al., 2003, PASP, 115, 453
Li W. et al., 2011, MNRAS, 412, 1441
Liu Z. W., Pakmor R., Röpke F. K., Edelmann P., Wang B., Kromer M., Hillebrandt W., Han Z. W., 2012, A&A, 548, A2
Livne E., Asida S. M., Höflich P., 2005, ApJ, 632, 443
Maund J. R. et al., 2010, ApJ, 722, 1162
Mazzali P. A., Lucy L. B., 1993, A&A, 279, 447
Mazzali P. A., Nomoto K., Patat F., Maeda K., 2001, ApJ, 559, 1047
Mazzali P. A., Röpke F. K., Benetti S., Hillebrandt W., 2007, Sci, 315, 825
McClelland C. M. et al., 2010, ApJ, 720, 704
Moriya T., Tominaga N., Tanaka M., Nomoto K., Sauer D. N., Mazzali P. A., Maeda K., Suzuki T., 2010, ApJ, 719, 1445
Nomoto K., Thielemann F.-K., Yokoi K., 1984, ApJ, 286, 644
Nonaka A., Aspden A. J., Zingale M., Almgren A. S., Bell J. B., Woosley S. E., 2012, ApJ, 745, 73
Osher S., Sethian J. A., 1988, J. Comput. Phys., 79, 12
Pakmor R., Kromer M., Taubenberger S., Sim S. A., Röpke F. K., Hillebrandt W., 2012, ApJ, 747, L10
Pan K.-C., Ricker P. M., Taam R. E., 2012, ApJ, 750, 151
Pastorello A. et al., 2007a, MNRAS, 377, 1531
Pastorello A. et al., 2007b, MNRAS, 376, 1301
Perlmutter S. et al., 1999, ApJ, 517, 565
Phillips M. M., 1993, ApJ, 413, L105
Phillips M. M. et al., 2007, PASP, 119, 360
Pickles A. J., 1998, PASP, 110, 863
Plewa T., Calder A. C., Lamb D. Q., 2004, ApJ, 612, L37
Pskovskii I. P., 1977, SvA, 21, 675
Reinecke M., Hillebrandt W., Niemeyer J. C., Klein R., Gröbl A., 1999, A&A, 347, 724
Riess A. G. et al., 1998, AJ, 116, 1009
Röpke F. K., 2005, A&A, 432, 969
Röpke F. K., Hillebrandt W., 2005, A&A, 431, 635
Röpke F. K., Woosley S. E., Hillebrandt W., 2007, ApJ, 660, 1344
Röpke F. K. et al., 2012, ApJ, 750, L19
Ruiter A. J., Belczynski K., Fryer C., 2009, ApJ, 699, 2026
Ruiter A. J. et al., 2012, arXiv:e-prints
Sahu D. K. et al., 2008, ApJ, 680, 580
Schmidt B. P. et al., 1998, ApJ, 507, 46
Schmidt W., Niemeyer J. C., Hillebrandt W., 2006a, A&A, 450, 265
Schmidt W., Niemeyer J. C., Hillebrandt W., Röpke F. K., 2006b, A&A, 450, 283
Seitenzahl I. R., Meakin C. A., Lamb D. Q., Truran J. W., 2009a, ApJ, 700, 642
Seitenzahl I. R., Meakin C. A., Townsley D. M., Lamb D. Q., Truran J. W., 2009b, ApJ, 696, 515
Seitenzahl I. R., Röpke F. K., Fink M., Pakmor R., 2010, MNRAS, 407, 2297
Seitenzahl I. R., Ciaraldi-Schoolmann F., Röpke F. K., 2011, MNRAS, 414, 2709
Seitenzahl I. R. et al., 2012, MNRAS, in press (arXiv:1211.3015)
Sim S. A., 2007, MNRAS, 375, 154
Sim S. A., Röpke F. K., Hillebrandt W., Kromer M., Pakmor R., Fink M., Ruiter A. J., Seitenzahl I. R., 2010, ApJ, 714, L52
Smiljanovski V., Moser V., Klein R., 1997, Combust. Theory Modelling, 1, 183
Stanishev V. et al., 2007, A&A, 469, 645
Stehle M., Mazzali P. A., Benetti S., Hillebrandt W., 2005, MNRAS, 360, 1231
Travaglio C., Hillebrandt W., Reinecke M., Thielemann F.-K., 2004, A&A, 425, 1029
Valenti S. et al., 2009, Nat, 459, 674
Wang L., Wheeler J. C., 2008, ARA&A, 46, 433
Woosley S. E., Kasen D., 2011, ApJ, 734, 38
Zingale M., Almgren A. S., Bell J. B., Nonaka A., Woosley S. E., 2009, ApJ, 704, 196

APPENDIX A: OBSERVATION LOG AND DATA REDUCTION OF NEAR-INFRARED SPECTRA

Five low-resolution NIR spectra of SN 2005hk were obtained at the Very Large Telescope (VLT)/ISAAC (Table A1). During each night when the SN was observed, one of the following bright stars Hip 1115, Hip 26093 or Hip 115347, all of spectral type B3V, was also observed close in time and airmass to the SN observations. Four different instrument settings were used to obtain wavelength coverage between 0.97 and 2.5 mm. The observations for each setting were reduced separately. The spectra from the different instrument settings that did not overlap were scaled so that the synthetic *J* and *H* photometry matched the observed one published by Phillips et al. (2007).

The observations were performed in ABBA sequences, where A and B denote two different positions along the slit. The images were biased and flat-field corrected, and trimmed. Because of the field distortion of ISAAC, spectra taken at two different slit positions are not parallel. Besides, the image of the slit is also curved. For the subsequent data reduction it was necessary to correct for these two effects. This was achieved with the TWODSPEC.LONGSLIT package in IRAF. The input data for deriving this correction were: (i) the arc-lamp spectra obtained during the nights when the SN was observed and (ii) special (STARTRACE) observations obtained by ESO twice per year and consisting of spectra of a bright star taken at 11 different positions along the slit. After applying the geometric distortion

Table A1. Log of the VLT/ISAAC NIR spectroscopy.

Date (UT)	JD	Phase (d)
2005-11-09	2 453 683.58	−1.4
2005-11-14	2 453 688.58	3.6
2005-11-17	2 453 691.58	6.6
2005-11-23	2 453 697.58	12.6
2005-12-07	2 453 711.58	26.6

correction the night sky lines were parallel to the image columns and the spectra to the image rows. Next, for each pair of AB images the B image was subtracted from the A image. The negative spectrum was shifted to the position of the positive one and subtracted from it, resulting in an image with the sum of the spectra but without the sky background. All such images were summed into a single image and the 1D spectra were then optimally extracted. We note that the optimal extraction algorithm has to be applied on images with the pixel levels in the form of actual detected counts, and so it does not work quite correctly if applied to background-subtracted images. Special care was thus taken to calculate the optimal extraction weights correctly. The wavelength calibration was done with arc-lamp spectra. Its accuracy was checked against the sky lines and small corrections were applied if necessary.

To remove the strong telluric absorption features, the SN spectra were divided by the high-signal-to-noise spectra of the B3V stars. To obtain the relative flux calibration, the result was multiplied by a model continuum spectrum for a B3V star. We used a model spectrum with $T_{\mathrm{eff}} = 18\,500$ K and $\log g = 4$ by R. Kurucz, available at http://kurucz.harvard.edu/. The residual features due to the hydrogen absorption lines of the B3V stars were removed by dividing the SN spectra by the composite spectrum for the B3V spectral type from Pickles (1998). The composite B3V spectrum was first normalized to the continuum and smoothed to the instrumental resolution of each of the four instrumental setups used.

APPENDIX B: GTC LATE-PHASE PHOTOMETRY

Deep *r*-band (Fukugita et al. 1996) images of the SN 2005hk explosion site with exposure times of 3×200 s were obtained at the GTC equipped with OSIRIS on UT 2012 July 20, 2443.5 d after *B*-band maximum. The images were debiased, flat-field corrected, astrometrically aligned and averaged. An image quality of 0.9 arcsec was measured from the full width at half-maximum of isolated stars. The photometric zero-point of the image was determined by comparing instrumental magnitudes of stellar objects with the apparent *r*-band magnitudes reported in the Sloan Digital Sky Survey (SDSS) Data Release 6 catalogue (Adelman-McCarthy et al. 2008). Since no source was visible at the position of SN 2005hk, we estimated the limiting magnitude in our image by measuring faint stellar sources in similar locations as SN 2005hk. The apparent magnitude of the faintest of these sources, $r = 25.68 \pm 0.41$, was then adopted as limiting magnitude for the remnant of SN 2005hk. Note that this is $\sim$3.9 mag fainter than the last (Bessell) *R*-band magnitude of SN 2005hk, taken 381.6 d after *B*-band maximum (Sahu et al. 2008). With a colour excess of $E(B-V)_{\mathrm{tot}} = 0.112$ mag and a distance modulus of $\mu = 33.46 \pm 0.27$ mag, our limiting apparent magnitude translates into a limiting absolute magnitude of $M_r = -8.08 \pm 0.49$.

This paper has been typeset from a TEX/LATEX file prepared by the author.